Chromophore Orientations in Surface Relief Gratings with Second-Order Nonlinearity as Studied by Confocal Polarized Raman Microspectrometry

F. Lagugné-Labarthet, J. L. Bruneel, V. Rodriguez, and C. Sourisseau*

LPCM, UMR 5803, CNRS, Université de Bordeaux 1, 351 cours de la Libération, 33405 Talence Cedex, France

Received: September 19, 2003; In Final Form: November 17, 2003

Diffraction gratings of medium and strong efficiency (≈10−25%) were first inscribed on thin films of p(DR1M-*co*-MMA) copolymer, with a 12% azo mole fraction, and p(DR1M) azobenzene homopolymer using interferences between two linearly polarized (p + p) coherent laser beams. Then, the gratings were wire-poled at $T \approx T_g - 30$ °C under an intense dc electric field, inducing a noncentrosymmetry to the embedded chromophores. The grating surface relief modulation was controlled by atomic force microscopy (AFM), and the optical properties were investigated using UV−vis spectroscopy and second harmonic generation (SHG) polarized measurements. In addition, confocal micro-Raman polarized experiments were performed on virgin (unpoled) gratings, on related poled gratings, and also on gratings inscribed into previously poled films. Using a rigorous treatment of the Raman intensity variations, the two even-parity order parameters or Legendre's polynomials, $\langle P_2 \rangle$ and $\langle P_4 \rangle$, are estimated in the depth and peak regions of the surface reliefs; the corresponding forms of the most probable chromophore orientation distribution functions are thus determined and compared in the various gratings. It is thus concluded that the chromophore distribution functions are generally broad with strong maxima near ±90° in the bottom regions, and they are bimodal and asymmetric with sharp maxima at ±56−60° in the peak regions. These orientational anisotropic properties are largely maintained during the poling process, and consequently, the final surface relief amplitudes do not show any significant change (±20 nm). Finally, for the highest efficiency poled gratings of the p(DR1M) homopolymer there appears a notable deficiency in the chromophore density in the vicinity of the peak regions, which could be related to the existence of an apparent new half-period structure as recently evidenced from SHG near-field scanning optical microscopic measurements.

I. Introduction

Many organic nonlinear optical compounds have stimulated wide interest for their large nonlinearity and high-speed response, and more recently, micro- and nanostructured materials with large second-order $\chi^{(2)}$ properties have found potential applications in photonics as fiber optic couplers, as Bragg filters, and as cavities in degenerate feedback lasers. In this context, special attention has been paid to side chain azobenzene polymers which are suitable candidates for second harmonic generation (SHG) devices, not only in waveguide structures in order to obtain short wavelength coherent light sources[1−4] but also in polarization holographic gratings in order to create periodic modulations of the $\chi^{(2)}$ property in polymer films and to separate automatically the second-harmonic wave from the fundamental one.[5−11] In fact, following the pioneering and independent works of Rochon and co-workers[12−14] and Tripathy and co-workers,[15−17] numerous studies on various polymer systems have already been performed by several groups[18−44] so that the direct recording of diffraction gratings on polymer films functionalized with azobenzene molecules is now extensively documented. It is well-known how to inscribe large surface relief (amplitude) gratings with good thermal stability, without any pre- or postprocessing, and how to obtain high diffraction efficiencies (η%) on the ±1 order (η is the intensity ratio of the ±1 diffracted order over the zero-order transmitted beam). This process generally leads to large surface relief modulations (SRMs) from a few hundred nanometers up to the micrometer scale, that is, up to twice the initial film thickness. However, as far as we know there have been few reports of $\chi^{(2)}$ gratings fabricated by electric poling, either after the SRM formation process or directly on the previously poled polymer films, despite the advantages and the necessity for polymer-based optical circuits; moreover, the mechanisms and dynamics of the orientational molecular motions involved in the formation of these electro-optical devices have not yet been determined.

The aim of this study is thus to prepare polar gratings with a spatial modulation of the second-order nonlinearity by using a high dc electric field wire-poling technique and to characterize the chromophore polar orientations by confocal polarized Raman microscopy. Furthermore, in a recent study one of us (F.L.-L.) has recently paid attention to the formation of various electrically poled holographic gratings on thin films of the p(DR1M) homopolymer, with diffraction efficiencies of 5.0%, 12%, and about 25% and to their nonlinear properties as studied by near-field SHG microscopy;[45] in particular, for the highest efficiency gratings the resulting $\chi^{(2)}$ patterns as detected by SHG near-field scanning optical microscopy (NSOM) exhibited a periodic

* Author to whom correspondence should be addressed. Fax: (33) 5 40 00 84 02. E-mail: c.sourisseau@lpcm.u-bordeaux1.fr.

10.1021/jp0368076 CCC: $27.50
Published on Web 01/03/2004

structure different from that of the topographical far-field atomic force microscopy (AFM) images. So, another goal of this study is to settle this apparent controversy and, as far as possible, to discriminate between several orientational molecular models that provide explanations of such a surprising result. To address this problem from the point of view of the chromophore orientational properties, we have thus made use of the confocal micro-Raman scattering spectrometry, which is known as a very sensitive nondestructive vibrational spectroscopic technique with high spectral and spatial resolution and which may provide a wealth of information about the orientational distribution functions of the azo chromophores.[27,30,31,46] In fact, we have recently demonstrated in several micro-Raman studies[27,30,31,46] that from an inspection of the polarized Raman scattering spectra one can get estimates of the two first-order parameters of even parity, $\langle P_2 \rangle$ and $\langle P_4 \rangle$, and determine the chromophore distribution functions in the different regions, depth and peak, of the SRM profiles.

This paper is organized as follows: In experimental Section II the materials and the grating inscription are first described; also, the main conditions for the high dc electric field poling, the spectroscopic linear (UV−vis) and nonlinear (SHG) measurements, and the polarized Raman confocal microscopic recordings are briefly discussed. In the main Section III the real-time diffraction efficiency curves, AFM images, spectroscopic characterizations, and polarized micro-Raman results are then successively discussed for gratings inscribed on thin films of the p(DR1M-*co*-MMA) copolymer and of the p(DR1M) homopolymer. In Section IV the theoretical Raman intensity expressions and the corrections applied in polarized micro-Raman studies are first recalled; then, the Raman intensity results are illustrated with nicely resolved Raman images of the scanned surfaces and interpreted in terms of the molecular orientations via the calculation of both order parameters, $\langle P_2 \rangle$ and $\langle P_4 \rangle$. By use of the "information entropy model"[47] the most probable distribution functions in the bottom and top regions of the SRM profiles are obtained and compared. Finally, in the Section V we draw several important conclusions concerning the comparative chromophore orientations when the poling process is carried out after the grating inscription and, conversely, when the grating inscription is performed on a previously poled film. We thus provide new information about the relative contributions of the birefringence and surface relief gratings and their possible constructive or destructive interferences, that is, about the topographical images as obtained from far-field and near-field optical measurements. This could open new routes to preserve polar patterns on the regularly modulated surfaces of these azo polymers and/or to duplicate gratings with a large $\chi^{(2)}$ nonlinearity; new promising applications could be developed as well.

II. Experimental Section

II.A. Materials and Grating Inscriptions. We have used the so-called p(DR1M-*co*-MMA) copolymer and the p(DR1M) homopolymer containing 12% and 100% molar fraction of the azobenzene DR1 derivative covalently bonded in the side chain position, respectively (see Scheme 1). Details about the synthesis and polymer characterization (T_g = 129 °C) can be found elsewhere.[48,49] Thin films were prepared by spin coating a solution of the polymer in chloroform on clean glass microscope slides and heating for 30 min at 120 °C. The thickness of the films and the grating topographic data (see below) were controlled by AFM in the contact mode (Thermomicroscope Research CP; the tip was an Ultralever 06B with a force constant F = 0.4 N/m). The thickness of all the studied films was equal to 400 ± 10 nm.

SCHEME 1: Chemical Formulas of the p(DR1M-*co*-MMA) Copolymer (x = 0.12) and of the p(DR1M) Homopolymer (x = 1.0) Systems

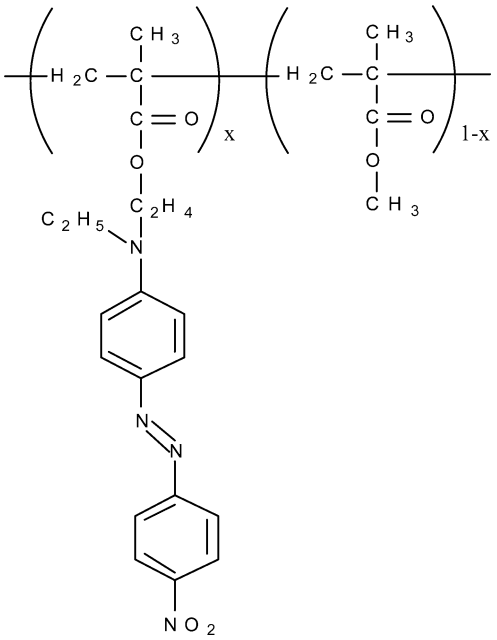

The holographic setup developed for the grating inscription has been already described.[32,50] Briefly, it consisted of a two-arm interferometer used to generate the interference pattern from an argon laser beam (λ = 514.5 nm) going through a Wollaston polarizer. The polarizations of the two emerging beams were adjusted using half-wave or quarter-wave retarder plates and carefully checked using a photopolarimeter (Thorlabs); the degree of linear polarization was always better than 98%. Both incident beams of equal intensity with an irradiance of about 30−40 mW/cm^2 (for each beam) were recombined onto the sample with an incidence angle (θ) equal to about ±10.8°. According to Bragg's law, $2\Lambda \sin(\theta) = \lambda$, the observed grating spacing was determined to be Λ = 1.373 μm. In all the experiments the time evolution of the transmitted and diffracted orders was probed using a linear vertically (s)-polarized He−Ne laser (λ_{probe} = 632.8 nm) with a very low intensity (I_{probe} < 0.05 mW). The probe beam was chopped at 1 kHz and impinged the thin film normal to its surface. Two identical photodiodes were used to probe simultaneously the intensity variations of the transmitted zero- and diffracted first-order signals, respectively, and the signals were demodulated using two lock-in amplifiers.

II.B. Optical Linear and Nonlinear Measurements. Wire poling under high-field conditions has been carried out using a tungsten wire (25 μm diameter) held parallel and above the films at a distance as short as 5 mm, to which a dc field of ≈3.0 kV was applied to ensure an efficient charge injection on the polymer surface.[51−53] The temperature of the poling process was relatively high (≈90 °C) to achieve good stability of the induced polar order but significantly below the T_g of the polymer (≈120−125 °C) to maintain a stable surface relief amplitude. The dc electric field was applied during a 1 h period in order to achieve an overall good structural polar ordering, and then each film was slowly cooled to room temperature at a rate of 1 °C/min with the dc field on to ensure freezing of the chromophore orientations.

The polarized UV−vis absorption spectra were recorded on a double-beam spectrometer (SAFAS, 190 DES, Monaco) systematically before and after the poling process, and a simple

glass slide was used on the reference beam. The efficiency of the poling was estimated by a comparison of the spectra before and after poling the film, allowing a crude determination of the axial order parameter along the film thickness (Z direction), under the uniaxial symmetry assumption:

$$\langle P_2 \rangle_Z = \frac{A_{\parallel} - A_{\perp}}{A_{\parallel} + 2A_{\perp}} \quad (1)$$

The SHG measurements were performed using the optical setup already described in a previous study.[54] Polarized (p−p) and (s−p) SHG Maker fringe patterns were recorded just after the poling process and later, from time to time, over a three month period; the symbols "p" and "s" indicate horizontal and vertical linear polarization, respectively. We have used a 1064 nm Nd:YAG laser operating at very low irradiance (pulse energy < 50 μJ, repetition rate of 200 Hz, and pulse width of 15 ns). A general SHG matrix method for multilayered anisotropic linear and nonlinear media has been applied allowing the determination of the resonance enhanced nonlinear d_{ij} coefficients (d_{33} and $d_{31} = d_{15}$, respectively), as well as the linear absorption coefficients at the harmonic wave (at 532 nm) and the average value of the $\langle P_2 \rangle$ orientational parameter with respect to the poling field direction.

The Raman spectra were recorded in the backscattering geometry on a Labram I (Jobin-Yvon, Horiba Group, France) microspectrometer in conjunction with a confocal microscope and a 100× objective lens; the optical setup has already been published.[27,30,46] To avoid any thermal, photochemical, or bleaching effects, we have used a minimum intensity power (≈0.75−1.50 mW) of the 752.5 nm incident line from an Ar−Kr laser. The linear polarization direction of the laser beam was fixed as a result of the configuration setup of the instrument, which contained a special notch filter (at 752.5 nm) that eliminated the low-frequency elastic and inelastic contributions. Polarization analyses were performed on the backscattered radiation with a polarizing analyzer in the vertical (V) or horizontal (H) position and a depolarization scrambler in front of the entrance slit of the monochromator; the alignment and calibration of these optical elements were checked by recording both the intense polarized Raman spectra of CCl_4 liquid and also the Raman responses of a similar but isotropic thin sample. The already inscribed 1.37 μm period grating was mounted on the XY-motorized microscope table with ±0.125 μm controlled step scan displacements along the $\vec{X}$ grating vector direction. Typically, $40 \times 3 = 120$ Raman spectra were collected over three lines at different Y coordinates, each line of 5.0 μm length, and the acquisition time was fixed at 5 s (or 10 s) per spectrum leading to a total run time of $120 \times 5 = 600$ s (or 1200 s). Each polarized Raman image for a selected wavenumber range (as discussed below) is thus the result of integrated intensity variations observed over 120 recorded spectra for the surface grating under inspection. Obviously, this implies a high quality and stability of the optical setup, which was controlled at any time by a TV monitor displaying the video white light image of the scanned surface. Finally, a high-grade sensitivity air-cooled charge-coupled device (CCD) detector was used for detection, allowing a simultaneous spectral dispersion (from a 600 grooves/mm grating) over a wide wavenumber range (of about 2000 cm^{-1}), and the Raman shift measurements (±3 cm^{-1}) were calibrated using plasma lines.

SCHEME 2: Surface Relief Profile and Components of the Incident Electric Field upon Grating Inscription Using the (p + p) Polarization Configuration of the Incident Laser Beams

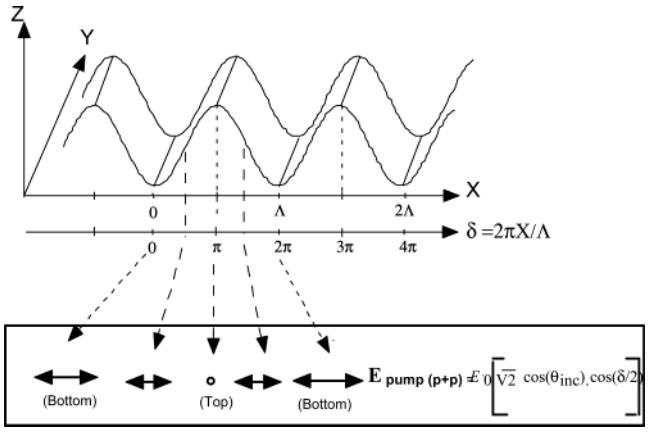

III. Diffraction Results, AFM Data, and Spectroscopic Characterizations

For gratings inscribed using the linear horizontal (p + p) polarization configuration, with respect to the grating $\vec{X}$ axis vector (horizontal) direction, the modulation of amplitude is important because the incident intensity varies between $\approx 2I_0$ and 0 over a half-period spacing (Scheme 2); this setup is reported as being very efficient for grating inscription,[23,24,31,55] and we have intentionally chosen this configuration to facilitate the further dye orientations during the poling. Under these conditions, we have first examined the real-time diffraction efficiency curves for the writing of some gratings with a medium efficiency (≈5.8−6.2%) on p(DR1M-*co*-MMA) thin films (Figure 1) and with a larger efficiency (≈21−25%) on p(DR1M) polymer films (Figure 2). In the former case, as shown in Figure 1, starting from an isotropic film we obtain a 6.2% diffraction efficiency after a 1100 s irradiation period, but a longer 2700 s period would lead to an increase up to $\eta \approx 22\%$. In contrast, when using an initially poled anisotropic film, the inscription kinetics is slower, and it takes a longer time of nearly 1400 s to reach about 5.8% of efficiency; this shows that the formation of the birefringence grating, which mimics the polarization pattern, and the development of the surface relief grating, which involves a significant mass transport, are rendered more difficult on a previously poled sample. In the latter case with the homopolymer p(DR1M) sample, as shown in Figure 2, higher diffraction gratings with an efficiency equal to 25% and 21% are inscribed on a virgin isotropic film (after a short irradiation period of 700 s) and on a previously poled film (after the longer period of 1200 s), respectively. Again, the dynamics of grating inscription is significantly slowed when using the poled film, but very importantly, we observe new pronounced variations at short times due first to the molecular reorientations and second to destructive interferences between the birefringence and surface relief contributions; finally, this anomaly is followed by an increase in the efficiency when the growth of the surface modulation becomes dominant (see the inset of Figure 2).

In the above-discussed gratings, the large surface relief sinusoidal modulations were controlled by AFM topographic measurements. In the first gratings on the copolymer film with 6.2% efficiency, a relief amplitude equal to 180 and 200 nm has been observed before and after a 1-h poling experiment, respectively (Figure 3a); this demonstrates that the polar ordering under an intense dc electric field does not destroy the grating

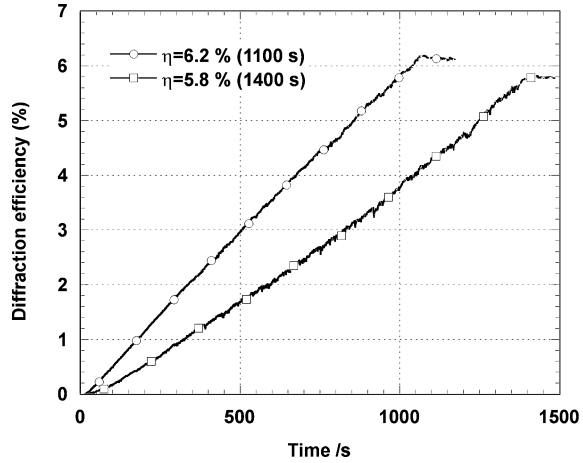

Figure 1. Real-time variations of the diffraction efficiency measured on the + first order for medium efficiency gratings inscribed on a 12% azo-containing copolymer film before poling ($\eta = 6.2\%$ for a writing period of 1100 s) and on a previously poled film ($\eta = 5.8\%$ for a writing period of 1400 s), respectively.

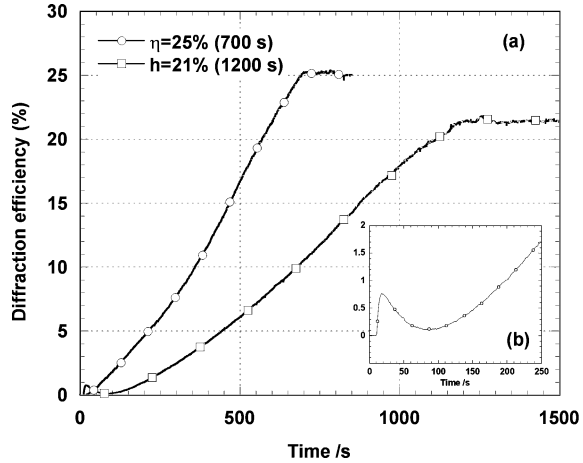

Figure 2. (a) Real-time variations of the diffraction efficiency measured on the + first order for high-efficiency gratings inscribed on a 100% azo-containing homopolymer film before poling ($\eta = 25\%$ for a writing period of 700 s) and on a previously poled film ($\eta = 21\%$ for a writing period of 1200 s), respectively. (b) The inset shows the drastic changes observed at short times in the latter case.

surface morphology; in contrast, a weak modulation increase of 20 nm is even noted, a result, however, in agreement with other studies on azobenzene-containing polyurethane films.[9,10] As expected, a similar relief amplitude equal to 175 nm was also detected for the grating($\eta \approx 5.8\%$) inscribed on the previously poled copolymer film.

Stronger relief modulations were observed for gratings inscribed on the p(DR1M) homopolymer film; for instance, a grating of ≈16% efficiency (for a laser writing period of ≈500 s) displayed a relief amplitude modulation equal to 290 and 310 nm before and after a 1-h poling experiment, respectively, as checked from AFM data (Figure 3b); we again note a 20 nm increase after the poling process under an intense dc electric field, although the temperature was raised to 90 °C. Also, the grating of 21% efficiency inscribed on the previously poled film exhibited an important relief amplitude as large as 390 nm, that is, nearly equal to the film thickness.

Furthermore, some linear (UV−vis) and nonlinear (SHG) spectroscopic characterizations were systematically performed on the film surfaces before and after the poling process; in these

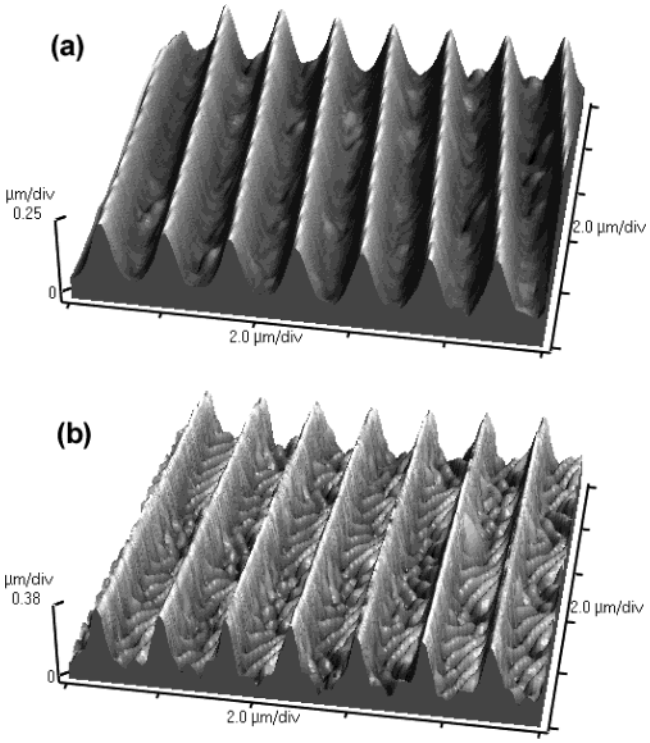

Figure 3. Topographic AFM results obtained (a) for a poled grating inscribed on a 12% azo-containing copolymer film ($\Delta h \approx 200$ nm) and (b) for another poled grating inscribed on a 100% azo-containing homopolymer film ($\Delta h \approx 304$ nm).

experiments, intentionally performed in the near vicinity of the grating location, we have measured the absorbance spectra (300−900 nm) and the polarized SHG Maker fringe responses. As shown in Figure 4a, the UV−vis spectra of a 12% azo-containing copolymer sample display an intense absorbance maximum at 471 nm before poling and a weaker red-shifted signal at 476 nm after poling; according to eq 1 and to the following general relation,

$$\langle P_2 \rangle_Z = 1 - \frac{A_\perp}{A_0} = 1 - \frac{3A_\perp}{A_{||} + 2A_\perp} = \frac{A_{||} - A_\perp}{A_{||} + 2A_\perp} \qquad (2)$$

this leads to a crude estimate of the $\langle P_2 \rangle_Z$ order parameter roughly equal to +0.270. Similarly, the UV−vis spectra of the homopolymer sample reported in Figure 5a display a strong absorbance maximum at 461 nm before poling and a less intense red-shifted signal at 467 nm after poling, leading to a $\langle P_2 \rangle_Z$ order parameter roughly equal to +0.225. In both cases, the large positive values of the order parameter confirm that the poling reaction was efficient and the dye chromophores were significantly reoriented in the direction of the imposed electric field (perpendicular to the film plane). As a matter of fact, as shown in Figures 4b and 5b the polarized (p−p) and (s−p) Maker fringe patterns recorded over a wide angular range (+80°, −80°) for the 1-h poled films display very intense (p−p) responses and drastically weaker (s−p) signals, respectively; the observed ratios $(I_{s,p}/I_{p,p})^{1/2}$ are lower than 0.33 (≈0.23−0.25), and they confirm that the poling has actually been realized under high-field conditions. Note that the SHG measurements were performed on a flat area close to the inscribed gratings. Moreover, a complete treatment of the whole SHG data following a recently published procedure[52,54] leads to large values of the d_{33} nonlinear optical (NLO) coefficient equal to ≈120 pm/V and ≈350 pm/V immediately after the poling of

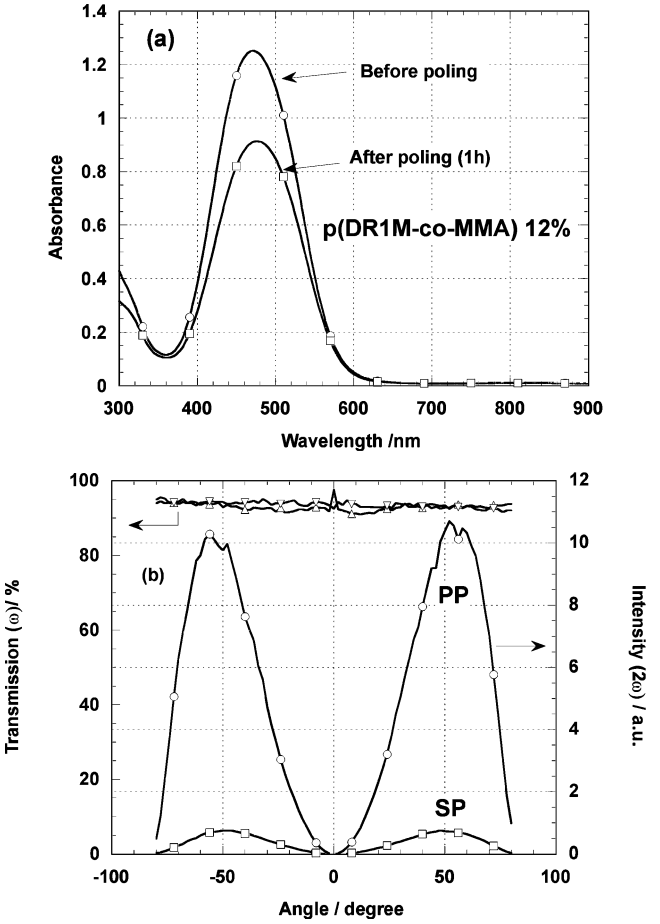

Figure 4. (a) Typical UV−vis absorption spectra (300−900 nm) and (b) transmission (p−p)- and (s−p)-polarized SHG responses, $I(2w)$, recorded over a wide angular domain (±80°) for a 12% azo-containing copolymer film after a 1-h wire-poling process under an intense dc electric field.

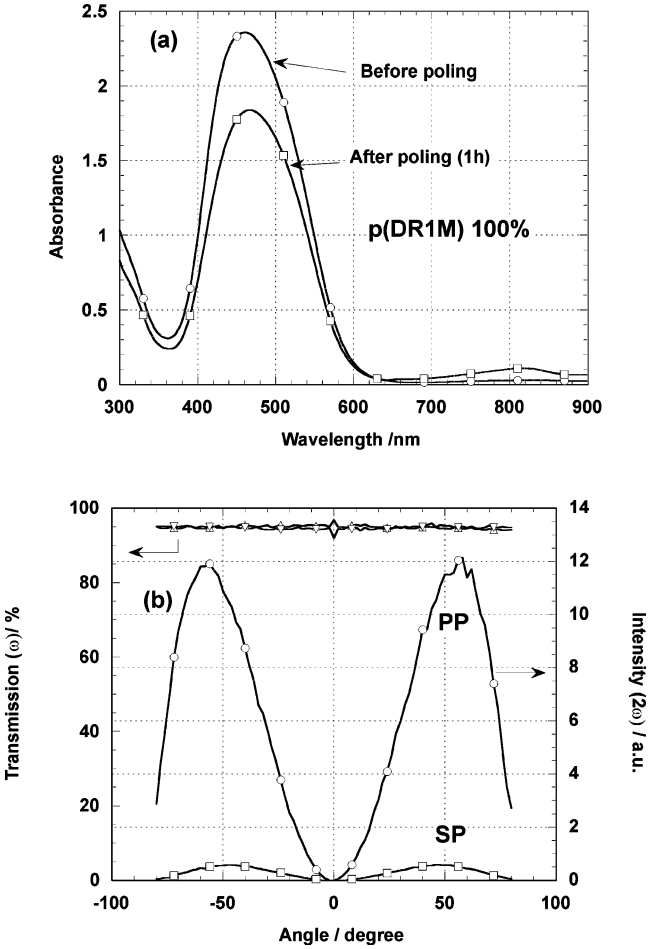

Figure 5. (a) Typical UV−vis absorption spectra (300−900 nm) and (b) transmission (p−p)- and (s−p)-polarized SHG responses, $I(2w)$, recorded over a wide angular domain (±80°) for a 100% azo-containing homopolymer film before and after a 1-h wire-poling process under an intense dc electric field.

the co- and homopolymer films, respectively (with respect to quartz with $d_{11} = 0.30$ pm/V). It must also be pointed out that, as expected, a slight decay of the second harmonic power was observed over time; nevertheless, the same films were still displaying intense SHG signals and d_{33} coefficients equal to ≈30 pm/V and ≈250 pm/V, respectively, after a 3 month period. No further decay at room temperature was observed for the 100% azo-containing polymer film, and its d_{33} NLO coefficient remains quite large; it compares favorably with the 102 pm/V value recently reported for a urethane−urea copolymer sample corona-poled at 150 °C by applying a dc electric field of 10 kV for 10 min.[5]

In conclusion, the above-characterized holographic gratings inscribed using the linear (p + p) incident polarization configuration and wire-poled under high dc electric field conditions appear to be fairly stable. The linear polarization configuration used seems appropriate for further dc poling perpendicular to the film plane, but the microscopic dye molecular orientational mechanisms are still open to discussion. It is thus the aim of our confocal microspectrometric Raman study to afford new information in that direction.

IV. Theoretical Intensity Expressions and Polarized Micro-Raman Results

IV.A. Theoretical Polarized Raman Intensity Expressions. Because of the cylindrical symmetry of the azobenzene chromophores, the molecular polarizability tensor is assumed to be diagonal:

$$\tilde{\tilde{\alpha}} = \begin{pmatrix} \alpha_1 & 0 & 0 \\ 0 & \alpha_1 & 0 \\ 0 & 0 & \alpha_3 \end{pmatrix} \quad (3)$$

Then, the molecular orientations in the grating are expected to derive primarily from the resulting electric field of the two (p + p) interfering incident beams (Scheme 2). According to recent theories of photoinduced anisotropy by a polarized laser beam and assuming that the angular density of "trans" chromophores is governed by the angular hole burning (AHB) process,[56−59] one may write in the weak pumping limit ($J \ll 1.0$),

$$n_T(\theta) \equiv \frac{N}{4\pi}(1 - J\cos^2\theta_p) \quad (4)$$

where θ_p is the angle between the pump polarization direction and the main long axis of the chromophore. So, as previously demonstrated for thin films irradiated under the same polarization condition and for gratings investigated in standard backscattering Raman experiments using an incident laser linearly polarized either in the parallel (Y) or in perpendicular (X)

direction (see the definition of axes in Scheme 2), the intensity expressions are[30,60]

$$I_{(YY)} = \frac{N}{105}\alpha_3^2\left[(21 + 28a_1 + 56a_1^2) - J\cos^2\left(\frac{\delta}{2}\right)(3 + 8a_1 + 24a_1^2)\right] \quad (5)$$

$$I_{(YX)} = I_{(XY)} = \frac{N}{105}\alpha_3^2\left[(7 - 14a_1 + 7a_1^2) - J\cos^2\left(\frac{\delta}{2}\right)(3 - 6a_1 + 3a_1^2)\right] \quad (6)$$

$$I_{(XX)} = \frac{N}{105}\alpha_3^2\left[(21 + 28a_1 + 56a_1^2) - J\cos^2\left(\frac{\delta}{2}\right)(15 + 26a_1 - 6a_1^2)\right] \quad (7)$$

where δ is the path difference between the two pump beams ($\delta = 2\pi X/\Lambda$) and $a_1 = \alpha_1/\alpha_3$ is the ratio of the molecular polarizability coefficients, which is expected to be very weak ($\ll$1.0) under preresonance Raman conditions. Therefore, to a first approximation, all the Raman intensity variations are expected to be in-phase and to display minima at $\delta = 0, 2\pi$ (bottom regions of the relief) and maxima at $\delta = \pi, 3\pi$ (top regions at half-period). It is noteworthy that the electric field is strictly zero at these latter positions, where the sample should normally remain isotropic. However, this is only a simple model and its spatial averaging assumes that all the chromophores undergo similar orientation effects whatever their original position; it is clear that the localized mass-transport and pressure effects on the polymer chains may also play a key role in the formation of the surface relief modulations, and they may perturb the initial dye molecular orientations.

In any way, from an experimental point of view we know that the very similar $I_{(YX)}$- and $I_{(XY)}$-polarized Raman spectra are generally less intense than the $I_{(YY)}$ and $I_{(XX)}$ ones and that the variations of both intensity ratios over a grating period,

$$R_1(\delta) = \frac{I_{(YX)}}{I_{(YY)}} \quad (8)$$

and

$$R_2(\delta) = \frac{I_{(XY)}}{I_{(XX)}} \quad (9)$$

will be mainly governed by those of the $I_{(YY)}$ and $I_{(XX)}$ denominators. Actually, it is also established that, because of the particular (p + p) incident polarizations used for grating inscription, the absorbances in the film plane will be largely anisotropic and stronger along the *Y* direction than along the *X* grating vector direction. So, in agreement with the previous studies of Zilker and co-workers,[41,61,62] the two above experimental ratios R_1 and R_2 must be corrected by the absorption term $(1 - e^{(-d/D)})$, where d is the film thickness ($d = 400$ nm) and D is the penetration depth at the 752.5 nm laser line ($D \approx 400$ nm); so, the ratios R_1 and R_2 were multiplied and divided by the factor 0.632, respectively. These treatments are very important because they will allow us to calculate the two first even-parity Legendre's polynomials, that is, the $\langle P_2\rangle$ and $\langle P_4\rangle$ order parameters of the chromophore in-plane orientational functions.

IV.B. Estimation of the $\langle P_2\rangle$ and $\langle P_4\rangle$ Coefficients in a Rigorous Treatment Taking into Account the Effect of the High Numerical Aperture Objective Lens. We consider now that all the photoinduced and mass-transport effects lead to the formation of anisotropic samples, but which keep a uniaxial symmetry around the pump laser polarization direction (*X* axis). To a first approximation, the angular distribution of the chromophores may be obtained by developing the function $f(\theta)$ on the basis of the first even-parity terms in the Legendre's polynomials:

$$\langle n_T\rangle = \frac{N}{4\pi^2}\int_0^{2\pi} d\psi \int_0^{2\pi} d\varphi \int_{-1}^{+1} f(\theta)\, d(\cos\theta)$$
$$= N\int_{-1}^{+1}\left[\frac{1}{2}\langle P_0\rangle P_0(\cos\theta) + \frac{5}{2}\langle P_2\rangle P_2(\cos\theta) + \frac{9}{2}\langle P_4\rangle P_4(\cos\theta)\right] d(\cos\theta) \quad (10)$$

where the coefficients $\langle P_l\rangle$ are the order parameters, which for full cylindrical symmetry are given by

$$\langle P_0\rangle = 1.0, \quad \langle P_2\rangle = \frac{1}{2}(3\langle\cos^2\theta\rangle - 1)$$

and

$$\langle P_4\rangle = \frac{1}{8}(35\langle\cos^4\theta\rangle - 30\langle\cos^2\theta\rangle + 3) \quad (11)$$

First of all, to compare the various polarized Raman intensities we have to calculate the polarizability tensor elements (in the laboratory frame) which are dependent on the following average quantities,

$$\langle\alpha_{IJ}^2\rangle = \langle[T(\theta,\varphi,\psi)\cdot\tilde{\alpha}T^t(\theta,\varphi,\psi)]^2\rangle \quad (12)$$

where $T(\theta,\varphi,\psi)$ (*or* T^t) is the Euler's angle transformation matrix (or transposed matrix).

Then, in a rigorous treatment we must take into account the effect of the high numerical aperture objective. In backscattering Raman microspectrometry it is well-known that analyses of polarization measurements can be established using the known optical properties of the wide aperture objective and the refractive index of the sample. On the basis of the results of Turrell and co-workers[63−65] and the use of the above-derived $\langle\alpha_{IJ}^2\rangle$ expressions (eq 12), in a first set of experiments we arrive at the general intensity equations

$$I_{(YX)} = [\langle\alpha_{YX}^2\rangle A + \langle\alpha_{YZ}^2\rangle B](2C_0 + C_2) + [\langle\alpha_{ZX}^2\rangle A + \langle\alpha_{ZZ}^2\rangle B](4C_1) + [\langle\alpha_{XX}^2\rangle A + \langle\alpha_{XZ}^2\rangle B](C_2) \quad (13)$$

$$I_{(YY)} = [\langle\alpha_{YY}^2\rangle A + \langle\alpha_{YZ}^2\rangle B](2C_0 + C_2) + [\langle\alpha_{ZY}^2\rangle A + \langle\alpha_{ZZ}^2\rangle B](4C_1) + [\langle\alpha_{XY}^2\rangle A + \langle\alpha_{XZ}^2\rangle B](C_2) \quad (14)$$

Similarly, in a second set of experiments (after a 90°rotation of the sample) we obtain

$$I_{(XY)} = [\langle\alpha_{XY}^2\rangle A + \langle\alpha_{XZ}^2\rangle B](2C_0 + C_2) + [\langle\alpha_{ZY}^2\rangle A + \langle\alpha_{ZZ}^2\rangle B](4C_1) + [\langle\alpha_{YY}^2\rangle A + \langle\alpha_{YZ}^2\rangle B](C_2) \quad (15)$$

$$I_{(XX)} = [\langle\alpha_{XX}^2\rangle A + \langle\alpha_{XZ}^2\rangle B](2C_0 + C_2) + [\langle\alpha_{ZX}^2\rangle A + \langle\alpha_{ZZ}^2\rangle B](4C_1) + [\langle\alpha_{YX}^2\rangle A + \langle\alpha_{YZ}^2\rangle B](C_2) \quad (16)$$

Here, the quantities *A* and *B* come from integrations of the squares of the electric vector components over the scattering

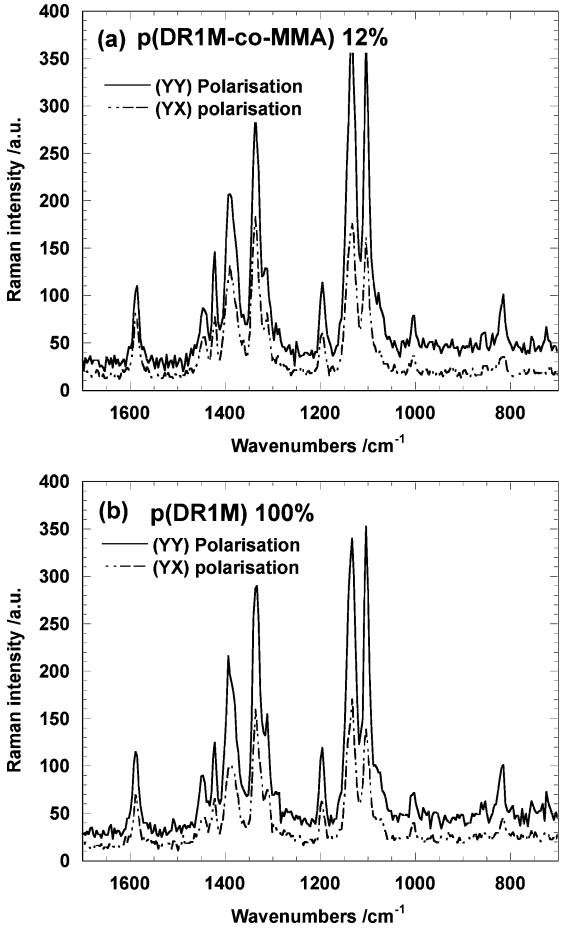

Figure 6. Typical survey (*YY*)- and (*YX*)-polarized (solid and dashed lines, respectively) Raman spectra in the 700−1700 cm^{-1} range recorded from the surface of (a) an electrically poled grating ($\eta = 6\%$) inscribed on a 12% azo-containing copolymer film and (b) another electrically poled grating ($\eta = 16\%$) inscribed on a 100% azo-containing homopolymer film.

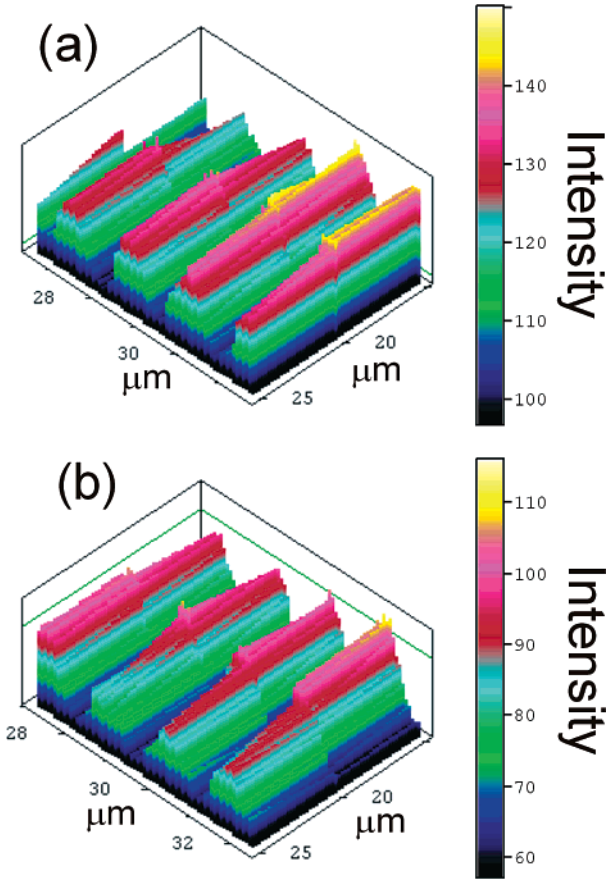

Figure 7. Three-dimensional plots of polarized Raman images from a 5 × 10 μm^2 area of an unpoled grating ($\eta = 22\%$) inscribed on a 12% azo-containing copolymer film and recorded using (a) (*YY*) and (b) (*YX*) polarization conditions.

cone and the coefficients C_0, C_1, and C_2 are related to the focalization efficiency, and they are calculated via integration of the incident electric field vector components over the effective irradiated volume. All these parameters are dependent on the angular semiaperture of the objective ($\theta_m = 64.16°$ for the 100× lens with a numerical aperture of 0.9) and the refractive index of the sample, n (at 752.5 nm). In the present study we have considered for the 12% (100%) azo-containing polymer sample with $n \approx 1.595$ ($n \approx 1.645$)[66] the parameter values of $A = 3.1599$ (2.9685) and $B = 0.5655$ (0.4956), and the numerically computed coefficients were found to be $C_0 = 5.5893$ (5.3825), $C_1 = 0.1566$ (0.1424), and $C_2 = 0.00117$ (0.00056), respectively.[67]

IV.C. Survey Raman Spectra. Using the 752.5 nm red laser line excitation, satisfactory fluorescence-free Raman results were first obtained for all polymer films, and some typical Raman results are reported in Figure 6; they demonstrate that very similar polarized spectra with good signal-to-noise ratios are observed for large efficiency grating samples ($\eta \approx 22-26\%$) inscribed (before any poling process) on either a copolymer (Figure 6a) or an homopolymer film (Figure 6b), respectively. The spectra recorded in the 700−1700 cm^{-1} wavenumber range exhibit intense bands at 1104 cm^{-1} ($\nu\Phi$−N, 18a), 1134 and 1196 cm^{-1} (δCH ring, 9a and 9b), 1336 cm^{-1} (ν_s NO_2), 1392 cm^{-1} (νN═N), 1422 and 1447 cm^{-1} (δCH ring, 19a and 19b), and 1572 and 1589 cm^{-1}(ωC═C, 8a and 8b) characteristic of the "trans" azobenzene chromophore;[60,68,69] in addition, the two couples of *YY*- and *YX*-polarized spectra display strong intensity variations confirming the existence of important orientational effects. In the following we have arbitrarily selected the whole 1044−1180 cm^{-1} spectral domain to perform the intensity integrations. Note that integrations of the single band ν_s NO_2 at 1336 cm^{-1} would give rise to similar results, but with a poorer signal-to-noise ratio.

IV.D. Polarization Analyses and Raman Images for an Unpoled Grating and Two Poled Gratings Inscribed on 12% Azo-Copolymer Thin Films. Here, as a reference sample we have used an unpoled grating of high diffraction efficiency ($\eta \approx 21\%$) obtained after a relatively long 2700 s writing period. Two series of typical polarized Raman spectra were recorded over the whole 200−1800 cm^{-1} range from a surface area of about 5 × 10 μm^2 using both the $Z(YY)\bar{Z}$ and $Z(YX)\bar{Z}$ scattering geometries in the first set of experiments and, similarly, both the $Z(XX)\bar{Z}$ and $Z(XY)\bar{Z}$ geometries in a second set. After intensity integrations, three-dimensional (3D) plots of the Raman intensity variations are built, and they lead to two couples of polarized Raman images as reported in Figures 7 and 8, respectively. These 3D plots nicely reproduce the ≈1.37 μm period spacing, and they show along the $X(\delta)$ direction large intensity variations, which are nearly in-phase, as expected, in all experiments. We thus conclude that the main orientational effects on the dye molecules are correctly predicted by the AHB model. More importantly, as shown in parts a and b of Figure 7 the Raman images exhibit large intensity contrasts between wide valleys and strong peaks, and the intensity variations in the slope regions are also well resolved. This demonstrates that

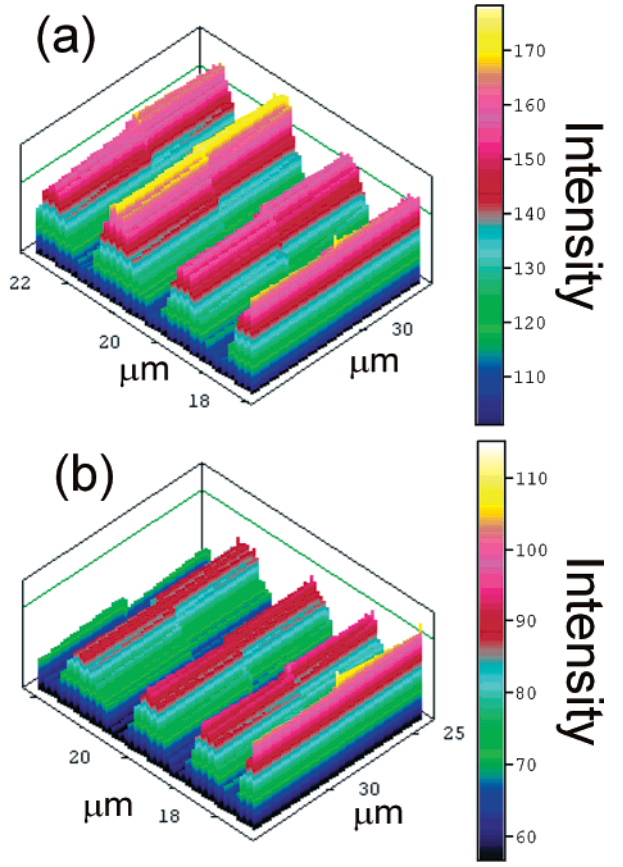

Figure 8. Three-dimensional plots of polarized Raman images from a 5 × 10 μm^2 area of an unpoled grating (η = 22%) inscribed on a 12% azo-containing copolymer film and recorded using (a) (*XX*) and (b) (*XY*) polarization conditions.

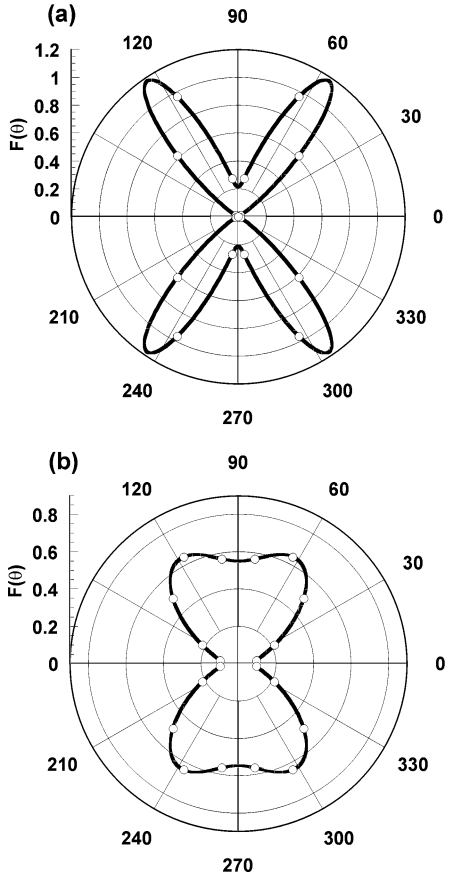

Figure 9. Polar representation of the chromophore distribution functions calculated at the (a) top and (b) bottom regions of the sinusoidal surface relief of an unpoled grating (η = 22%) inscribed on a 12% azo-containing copolymer film.

we are actually working at the diffraction limit because a quarter period (≈0.342 μm) is roughly equal to the half wavelength, $\lambda/2$ (0.376 μm).

The Raman intensities observed at each ±0.125 μm sample displacement along the *X* direction are then analyzed; these intensity variations are averaged over the three scanned lines and the values of the $R_1(\delta)$ and $R_2(\delta)$ ratios are obtained (Table 1). Even though there were some dispersed and scattered points, we found in these treatments that the ratios are always maximizing at the top regions of the surface relief. Actually, the $R_1(\delta)$ and $R_2(\delta)$ ratios are varying from the bottom ($X = 0$) to the top ($X = \Lambda/2$) regions over the 0.34−0.44 and 0.62−0.89 ranges, respectively; this indicates that the orientational order parameters $\langle P_2 \rangle$ and $\langle P_4 \rangle$ are also varying along a grating period. Under these conditions, with the use of the theoretical intensity expressions (see eqs 13−16), estimates of the $\langle P_2 \rangle$ and $\langle P_4 \rangle$ coefficients were calculated (Table 1). First, it must be pointed out that at the $X = 0$, Λ (bottom) positions, where the incident electric field was maximum, the values of the $\langle P_2 \rangle$ and $\langle P_4 \rangle$ order parameters are equal to −0.125, and −0.047, respectively. In addition, at the $X = \Lambda/2$ (top) positions the $\langle P_2 \rangle$ value is again negative, −0.108, and the $\langle P_4 \rangle$ order parameter is more significant, −0.188. We thus conclude that the principal long axis of the azobenzene molecules is always reorientated perpendicularly to the electric field of the actinic light, but the orientational effects appear more pronounced in the bottom regions. Nevertheless, the related $\langle P_2 \rangle$ values are very far from the −0.5 limit expected for a complete ordering of all the chromophores, and their orientations are probably spread over a wide domain.

Now, from the knowledge of the two first even-parity order parameters we are able to estimate the most probable orientational distribution functions, $f(\theta)$, by utilizing the "information entropy theory".[47,70−72] In this approach the distribution function is obtained by maximizing the information entropy, and the Lagrange method of undetermined multipliers leads to the function

$$f(\theta) = Z^{-1} \exp[\lambda_2 P_2(\cos\theta) + \lambda_4 P_4(\cos\theta)] \qquad (17)$$

where λ_2 and λ_4 are the Lagrange multipliers and *Z* denotes a normalization constant,

$$Z = \int_{-1}^{+1} \mathrm{d}(\cos\theta) \exp[\lambda_2 P_2(\cos\theta) + \lambda_4 P_4(\cos\theta)] \qquad (18)$$

Therefore, λ_2 and λ_4 were numerically calculated, and their values are reported in Table 1; the corresponding normalized functions $f(\theta)$ are thus obtained, and their plots in a polar coordinate representation are shown in Figure 9. These distributions differ drastically: in the bottom regions, a major fraction of the probed molecules are oriented nearly perpendicularly to the actinic light, but we observe a broad asymmetric function with the more intense maxima at ±62°; in contrast, in the peak regions the distribution is really bimodal asymmetric, and sharp maxima at ±56° are clearly evidenced. So, in agreement with previous Raman studies[27,30,46] we arrive at the conclusion that, because of pressure and force gradient effects during the isomerization cycles and the related mass-transport processes, the chromophore orientation distributions are perturbed (mainly in the peak regions) by the formation of the large surface relief modulation.

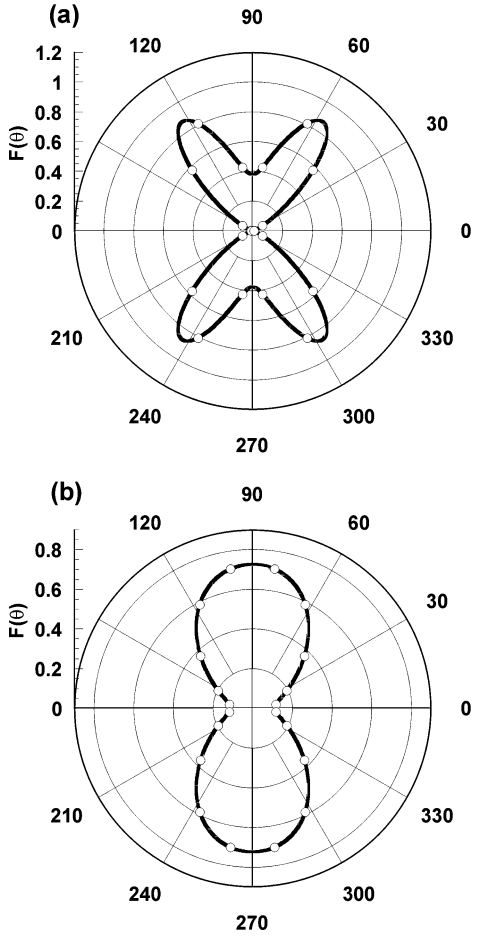

Figure 10. Polar representation of the chromophore distribution functions calculated at the (a) top and (b) bottom regions of the sinusoidal surface relief of a poled grating ($\eta \approx 6\%$) inscribed on a 12% azo-containing copolymer film.

As a second test grating sample we have intentionally used a 1-h poled sample of weaker diffraction efficiency ($\eta \approx 6.2\%$) in order to work with a less-pronounced amplitude of the surface relief ($\Delta h = 190$ nm). Similarly, two series of typical polarized Raman spectra were recorded from a surface area of about 5×10 μm^2 using the same scattering geometries as above, and similarly, four 3D plots of the integrated Raman intensity variations were obtained (not shown). Data treatments lead to new $R_1(\delta)$ and $R_2(\delta)$ ratio values, which are now varying between the bottom ($X = 0$) and top ($X = \Lambda/2$) regions over the 0.29−0.38 and 0.64−0.80 ranges, respectively; then, the $\langle P_2 \rangle$ and $\langle P_4 \rangle$ order parameters are equal to −0.177 and +0.007 at the bottom positions and −0.131 and −0.121 in the top regions, respectively (Table 1). Here, the $\langle P_2 \rangle$ parameter exhibits more significant negative values, whereas the $\langle P_4 \rangle$ order parameter remains important only at the top positions. Finally, the shapes of the new distribution functions are calculated and shown in Figure 10. In the bottom regions the function exhibits strong maxima at ±90° demonstrating that a very large fraction of the probed molecules are oriented perpendicularly to the actinic light; in the peak regions we still observe a bimodal asymmetric distribution with sharp maxima at ±57°. We thus arrive at the surprising conclusion that after a wire-poling process the distribution functions probed in the grating plane appear to be more confined in space at the bottom regions but somewhat broader with a slight decrease in the amplitude at the peak positions of the surface relief; nevertheless, we do not observe drastic orientational changes, a result in agreement with the persistent surface modulation.

Finally, as a third grating sample we have used a grating of similar weak diffraction efficiency ($\eta \approx 5.9\%$) and moderate surface relief modulation ($\Delta h = 174$ nm) but which was inscribed on a previously 1-h poled thin film. Similar polarized micro-Raman experiments were recorded and identical data treatments were performed to get the $R_1(\delta)$ and $R_2(\delta)$ ratios, the $\langle P_2 \rangle$ and $\langle P_4 \rangle$ order parameters, and the values of the λ_2 and λ_4 Lagrange multipliers. The main results are reported in Table 1, and they nicely compare to those obtained in the previous case. So, the final shapes of the distribution functions appear very similar; we thus conclude that even though the grating inscription process on an already poled film is more energy consuming, the distribution functions of the chromophores in various regions of the grating are similar, that is, they display strong maxima in the perpendicular direction at the bottom regions and a bimodal asymmetric shape with a weaker amplitude at the peak positions. It must be pointed out that, under the assumption of similar distributions in the third spatial direction (uniaxial model), the above results could allow the suggestion of the existence of a marked chromophore density deficiency at the exact peak maxima of the surface relief gratings.

IV.E. Polarization Analyses and Raman Images for an Unpoled Grating and Two Poled Gratings Inscribed on 100% Azo-Containing Polymer Thin Films. The first reference homopolymer thin film sample is now an unpoled high-efficiency grating ($\eta \approx 25\%$) obtained after a short (700 s) writing period. Two series of polarized micro-Raman spectra were again recorded on a 5×10 μm^2 surface area, and 3D plots of the Raman intensity variations leading to nicely resolved Raman images were obtained (not shown). It is noteworthy that the $R_1(\delta)$ and $R_2(\delta)$ ratios are now varying over different restricted domains, namely, over the 0.30−0.42 and 0.73−1.04 ranges for the bottom and top positions, respectively; also, the ratio values are always maximizing in the top regions, and the $R_2(\delta)$ value corrected from absorption effects becomes slightly larger than 1.0 (Table 2). These results indicate that the orientational order parameters $\langle P_2 \rangle$ and $\langle P_4 \rangle$ vary along a grating period, and finally, as compared with the first unpoled grating of the 12% copolymer sample, more negative values of the $\langle P_2 \rangle$ parameters but similar $\langle P_4 \rangle$ coefficients are obtained. Indeed, at the $X = 0$, Λ (bottom) positions, where the incident electric field was maximum, values of the $\langle P_2 \rangle$ and $\langle P_4 \rangle$ order parameters are equal to −0.181 and −0.023, respectively, and at the $X = \Lambda/2$ (top) positions the parameters are equal to −0.139 and −0.190, respectively (Table 2); once again, the chromophore orientations appear more pronounced in the bottom regions. Under these conditions the corresponding distribution functions are found to be relatively broad and asymmetric with maxima at ±71° in the bottom positions (Figure 11 b), and also bimodal asymmetric in shape with sharp maxima at ±58° in the peak regions (Figure 11a). In the latter case, the initial perpendicular orientations of the chromophores have been strongly perturbed by the formation of the large amplitude sinusoidal relief surface ($\Delta h \approx 430$ nm).

As a second test grating sample we have used a 1-h poled grating of significant diffraction efficiency ($\eta \approx 16.0\%$) but with a less pronounced surface relief ($\Delta h = 190$ nm). Similarly, nicely resolved polarized Raman images were obtained from a small surface area (not shown). The corresponding $R_1(\delta)$ and $R_2(\delta)$ ratio values are varying between the bottom ($X = 0$) and top ($X = \Lambda/2$) positions over the ranges of 0.31−0.39 and 0.70−1.04, respectively, that is, over similar domains as those previously observed for the unpoled grating. Consequently,

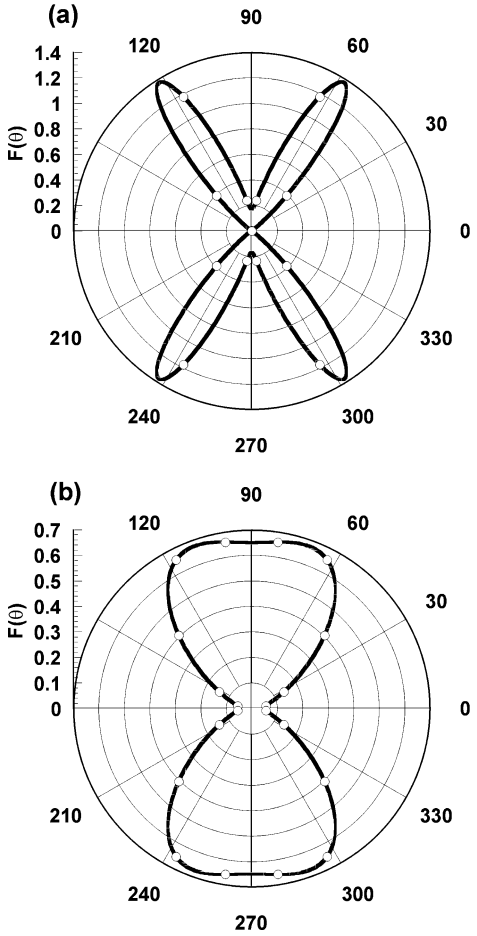

Figure 11. Polar representation of the chromophore distribution functions calculated at the (a) top and (b) bottom regions of the sinusoidal surface relief of an unpoled grating ($\eta = 25\%$) inscribed on a 100% azo-containing homopolymer p(DR1M) film.

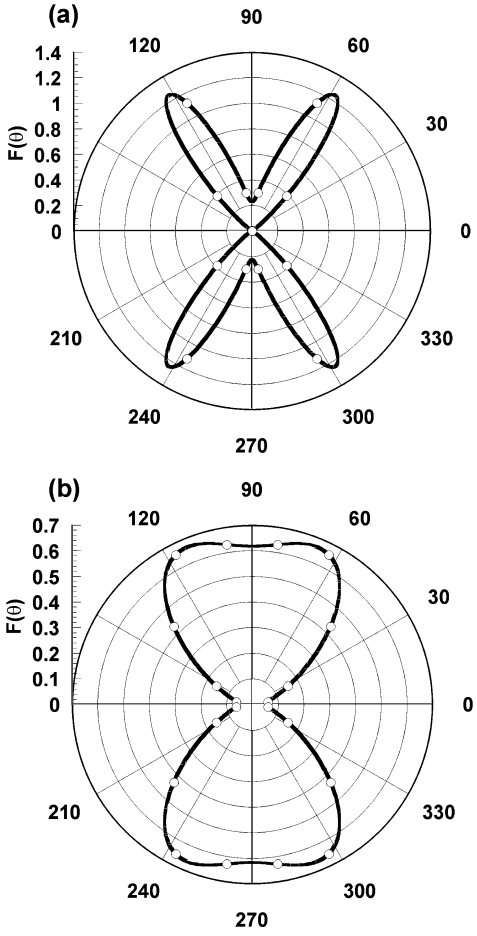

Figure 12. Polar representation of the chromophore distribution functions calculated at the (a) top and (b) bottom regions of the sinusoidal surface relief of a poled grating ($\eta \approx 16\%$) inscribed on a 100% azo-containing homopolymer p(DR1M) film.

values of the negative $\langle P_2 \rangle$ and $\langle P_4 \rangle$ order parameters are very similar and are equal to -0.167 and -0.032 at the bottom positions and -0.155 and -0.165 at the top regions, respectively (Table 2). Finally, as shown in Figure 12, the shapes of the distribution functions are again found to be relatively broad and asymmetric with maxima at $\pm 67°$ in the bottom positions, whereas they are bimodal and asymmetric in shape with sharp maxima at $\pm 58°$ in the peak regions. As compared with the above results, we conclude that during the poling process the initial chromophore orientations have not at all been perturbed. This corroborates the weak increase already noted in the amplitude of the relief modulation ($\Delta h \approx 190 \pm 20$ nm); we do not observe drastic orientational changes because of the persistent surface modulation.

Finally, as a third comparative sample we have used a grating with again a strong diffraction efficiency ($\eta \approx 21.5\%$) and a large surface relief modulation ($\Delta h \approx 390$ nm) but which was inscribed on a previously poled thin film. Similar polarized micro-Raman experiments were carried out and identical data treatments were performed in order to get the $R_1(\delta)$ and $R_2(\delta)$ ratios, the $\langle P_2 \rangle$ and $\langle P_4 \rangle$ order parameters, and the values of the λ_2 and λ_4 Lagrange multipliers. The main results are reported in Table 2 where they can be well compared to those obtained in the previous case, even though the $\langle P_2 \rangle$ negative coefficients are somewhat larger. So, the final shapes of the distribution functions are not drastically different, but in general, they are narrower; as compared with results for the 12% azo-containing films, quite similar conclusions can be drawn for the poled gratings of the homopolymer, and very importantly, we conclude that bimodal asymmetric chromophore distributions with a slightly weaker amplitude always take place at the peak positions of the sinusoidal surface relief. This phenomenon appears amplified in the higher diffraction gratings, and under the assumption of similar distributions in the third direction (Z), this could suggest an actual chromophore density deficiency in the near vicinity of the peak maxima of the surface relief gratings.

The above results can be favorably compared with recent data obtained from nonlinear measurements under scanning optical near-field microscopic conditions.[45,73] Indeed, SHG measurements conducted in both far-field diffraction and near-field microscopy have revealed the presence of an optical $\chi^{(2)}$ substructure in the SHG images, in particular in the top regions of the surface gratings inscribed on p(DR1M) films. The authors have tentatively assigned these splittings at the top regions to a variation in the viscoelastic properties of the polymer during the photofabrication of the surface relief. As the poling process is less efficient in the ridges of the grating, where the density of the material is weaker, the near-field SHG optical images display less intense SHG signals in these areas; this phenomenon was amplified in gratings with the largest surface relief amplitudes, because the changes in the viscoelastic properties were more pronounced. In agreement with results of the above Raman measurements, a deficiency in the density of chromophores oriented along the Z direction could also be related to a weaker SHG signal in the top regions. For the p(DR1M) gratings

TABLE 1: Final Values of the Order Parameters $\langle P_2 \rangle$ and $\langle P_4 \rangle$ and of Lagrange Multipliers λ_2 and λ_4, According to the "Information Entropy Theory", in the Various Regions of the Surface Relief of Three Gratings Inscribed on Thin Films of p(DR1M-*co*-MMA) with a 12% Azo Mole Fraction

	(p + p) polarization configuration						initial	
position (X)	R_1	R_2	$\langle P_2 \rangle$	$\langle P_4 \rangle$	λ_2	λ_4	incident field	distribution function
(a) $\eta = 21\%$ (after 2700 s): Unpoled Grating								
0.0 (bottoms)	0.341	0.625	−0.125	−0.047	−0.921	−0.749	↔	broad asymmetric (±62°)
$\Lambda/2$ (tops)	0.439	0.891	−0.108	−0.188	−2.799	−4.059	°	bimodal asymmetric maxima ±56°
(b) $\eta = 6.2\%$ (after 1050 s): Grating Poled during 1 h								
0.0 (bottoms)	0.286	0.643	−0.177	+0.0074	−1.150	−0.246	↔	strong maxima ±90°
$\Lambda/2$ (tops)	0.381	0.802	−0.131	−0.121	−1.752	−2.221	°	bimodal asymmetrical maxima ±57°
(c) $\eta = 5.9\%$ (after 1400 s): Grating Inscribed on a 1-h Poled Film								
0.0 (bottoms)	0.258	0.521	−0.174	+0.063	−0.926	+0.479	↔	strong maxima ±90°
$\Lambda/2$ (tops)	0.348	0.753	−0.147	−0.079	−1.458	−1.465	°	bimodal asymmetric maxima ±59°

TABLE 2: Final Values of the Order Parameters $\langle P_2 \rangle$ and $\langle P_4 \rangle$ and the Lagrange Multipliers λ_2 and λ_4 According to the "Information Entropy Theory" in the Various Regions of the Surface Relief of Three Gratings Inscribed on Thin Films of the p(DR1M) Homopolymer

	(p + p) polarization configuration						initial	
position (X)	R_1	R_2	$\langle P_2 \rangle$	$\langle P_4 \rangle$	λ_2	λ_4	incident field	distribution function
(a) $\eta = 25\%$ (after 700 s): Unpoled Grating								
0.0 (bottoms)	0.296	0.726	−0.181	−0.023	−1.415	−0.755	↔	broad asymmetric (±71°)
$\Lambda/2$ (tops)	0.416	1.042	−0.139	−0.190	−5.179	−6.036	°	bimodal asymmetric maxima ±58°
(b) $\eta = 16\%$ (after 500 s): Grating Poled during 1 h								
0.0 (bottoms)	0.307	0.701	−0.167	−0.0318	−1.297	−0.786	↔	broad asymmetric (±67°)
$\Lambda/2$ (tops)	0.390	1.045	−0.155	−0.165	−4.735	−5.229	°	bimodal asymmetric maxima ±58°
(c) $\eta = 21.5\%$ (after 1200 s): Grating Inscribed on a 1-h Poled Film								
0.0 (bottoms)	0.258	0.677	−0.208	+0.030	−1.351	−0.088	↔	strong maxima ±90°
$\Lambda/2$ (tops)	0.346	1.033	−0.183	−0.117	−3.851	−3.791	°	bimodal asymmetric maxima ±60°

with a high diffraction efficiency this is actually observed in Figures 11a and 12a, where the distribution functions are bimodal; similar observations were made in the copolymer films. We thus conclude that only a small fraction of chromophores are oriented in the exact Z direction (90°) in the ridges of the gratings; this occurs in both types of gratings, inscribed either before or after wire poling, and suggests that the number density of chromophores does not change significantly during the poling process.

Our Raman results are thus in keeping with the SHG measurements, and they confirm that the presence of $\chi^{(2)}$ substructure could originate in the grating inscription and not come from the poling process. However, because Raman intensities are only sensitive to even-parity $\langle P_2 \rangle$ and $\langle P_4 \rangle$ parameters, we cannot discriminate the polar orientation of the chromophores in a grating inscribed before or after poling. In contrast, SHG intensities are dependent on the odd-parity $\langle P_1 \rangle$ and $\langle P_3 \rangle$ order parameters, and it has been shown that gratings inscribed after poling of a flat polymer film were poorly active NLO materials, whereas those inscribed before poling displayed a large $\chi^{(2)}$ nonlinear susceptibility.[45,73] This can be rationalized in the first case by a random orientation of the polarly aligned chromophores upon irradiation by the actinic (p + p) polarized field. From such comparative results it is emphasized that Raman and NLO techniques (such as SHG or sum frequency generation spectroscopy (SFG)) are complementary means to characterize the anisotropy in such molecular systems and to determine their full orientational molecular distribution functions, considering the whole even and odd order parameter values up to $\langle P_4 \rangle$. Such works are in progress on these grating systems, and they will be published in a near future.

V. Conclusions

In the present study we have prepared polar gratings with a large spatial modulation of the surface relief and second-order nonlinearity properties from thin films of a 12% or 100% azo-containing p(DR1M) polymer. The chromophore orientations were investigated by confocal polarized Raman microscopic measurements and compared in unpoled or poled holographic gratings inscribed either before or after a wire-poling process under intense dc electric field. We have thus been able to determine the orientational distribution functions of the chromophores in any region, well and peak, of the surface reliefs. Also, in conjunction with AFM topographic data, for the first time we afford new information at the molecular level about the relative contributions of the phase (birefringence) and amplitude (surface modulation) effects in the poled gratings.

Finally, as compared with recent near-field SHG microscopic measurements performed on similar poled samples, we suggest that the superimposed additional periodic structures detected in NSOM on the $\chi^{(2)}$ patterns of the highest efficiency gratings could be due to a deficiency in the chromophore density near the peak maxima. It turns out that the (p + p) incident beam polarization configuration used in this study is actually very efficient not only for grating inscription but also for further polar ordering under an intense dc electric field. This could open new routes in various applications involving such electro-optic devices.

Acknowledgment. The authors are indebted to the CNRS (Chemistry Department) and to Région Aquitaine for financial support for the AFM and micro-Raman equipment. They are very thankful to A. Natansohn, Queen's University, Ontario (Canada) for providing the functionalized polymer samples and to F. Adamietz (LPCM) for valuable assistance in the poling experiments and SHG spectral recordings.

References and Notes

(1) Prasad, P. N.; Williams, D. J. In *Introduction to Nonlinear Optical Effects in Molecules and Polymers*; John Wiley & Sons: New York, 1991.

(2) Chemla, D. S.; Zyss, J. In *Nonlinear Optical Properties of Organic Molecules and Crystals*; Chemla, D. S., Zyss, J., Eds.; Academic Press: New York, 1986; Vol. 1.

(3) Boyd, R. W. In *Nonlinear Optics*; Academic Press: New York, 1992.
(4) Izawa, K.; Okamoto, N.; Sugihara, O. *Jpn. J. Appl. Phys.* **1993**, *32*, 807.
(5) Che, Y.; Sugihara, O.; Egami, C.; Fujimura, H.; Kawata, Y.; Okamoto, N.; Tsuchimori, M.; Watanabe, O. *Jpn. J. Appl. Phys.* **1999**, *38*, 6316.
(6) Toussaere, E.; Labbé, P. *Opt. Mater.* **1999**, *12*, 357.
(7) Martin, G.; Toussaere, E.; Soulier, L.; Zyss, J. *Synth. Met.* **2002**, *127*, 49.
(8) Martin, G.; Toussaere, E.; Soulier, L.; Zyss, J. *Synth. Met.* **2002**, *127*, 105.
(9) Munakata, K.; Harada, K.; Yoshikawa, N.; Itoh, M.; Umegaki, S.; Yatagai, T. *Opt. Rev.* **1999**, *6*, 518.
(10) Munakata, K.; Harada, K.; Anji, H.; Itoh, M.; Yatagai, T.; Umegaki, S. *Opt. Lett.* **2001**, *26*, 4.
(11) Blinov, L. M.; Palto, S. P.; Yudin, S. G.; De Santo, M. P.; Cipparrone, G.; Mazulla, A.; Barberi, R. *Appl. Phys. Lett.* **2002**, *80*, 16.
(12) Rochon, P.; Mao, J.; Natansohn, A.; Batalla, E. *Polym. Prepr.* **1994**, *35*, 154.
(13) Rochon, P.; Batalla, E.; Natansohn, A. *Appl. Phys. Lett.* **1995**, *66*, 136.
(14) Barrett, C. J.; Natansohn, A. L.; Rochon, P. L. *J. Phys. Chem. B* **1996**, *100*, 8836.
(15) Kim, D. Y.; Tripathy, S. K.; Li, L.; Kumar, J. *Appl. Phys. Lett.* **1995**, *66*, 1166.
(16) Kim, D. Y.; Li, L.; Jiang, X. L.; Shivshankar, V.; Kumar, J.; Tripathy, S. K. *Macromolecules* **1995**, *28*, 8835.
(17) Jiang, X. L.; Li, L.; Kumar, J.; Kim, D. Y.; Shivshankar, V.; Tripathy, S. K. *Appl. Phys. Lett.* **1996**, *68*, 2618.
(18) Barrett, C. J.; Rochon, P. L.; Natansohn, A. L. *J. Chem. Phys.* **1998**, *109*, 1505.
(19) Chen, J. P.; Lagugné-Labarthet, F.; Natansohn, A.; Rochon, P. *Macromolecules* **1999**, *32*, 8572.
(20) Yager, K. G.; Barrett, C. J. *Curr. Opin. Solid State Mater. Sci.* **2001**, *5*, 487.
(21) Natansohn, A.; Rochon, P. *Chem. Rev.* **2002**, *102*, 4139.
(22) Bian, S.; Liu, W.; Williams, J. M.; Samuelson, L.; Kumar, J.; Tripathy, S. K. *Chem. Mater.* **2000**, *12*, 1585.
(23) Tripathy, S. K.; Viswanathan, N. K.; Balasubramanian, S.; Kumar, J. *Polym. Adv. Technol.* **2000**, *11*, 570.
(24) Naydenova, I.; Nikolova, L.; Todorov, T.; Holme, N. C. R.; Ramanujam, P. S.; Hvilsted, S. *J. Opt. Soc. Am. B* **1998**, *15*, 1257.
(25) Pedersen, M.; Johansen, P. M.; Holme, N. C. R.; Ramanujam, P. S.; Hvilsted, S. *Phys. Rev. Lett.* **1998**, *80*, 89.
(26) Lagugné-Labarthet, F.; Buffeteau, T.; Sourisseau, C. *J. Phys. Chem. B* **1998**, *102*, 2654.
(27) Lagugné-Labarthet, F.; Buffeteau, T.; Sourisseau, C. *J. Phys. Chem. B* **1998**, *102*, 5754.
(28) Lagugné-Labarthet, F.; Buffeteau, T.; Sourisseau, C. *J. Phys. Chem. B* **1999**, *103*, 6690.
(29) Lagugné-Labarthet, F.; Rochon, P.; Natansohn, A. *Appl. Phys. Lett.* **1999**, *75*, 1377.
(30) Lagugné-Labarthet, F.; Bruneel, J. L.; Buffeteau, T.; Sourisseau, C.; Huber, M. R.; Zilker, S. J.; Bieringer, T. *Phys. Chem. Chem. Phys.* **2000**, *2*, 5154.
(31) Lagugné-Labarthet, F.; Bruneel, J. L.; Sourisseau, C.; Huber, M. R.; Bôrger, V.; Menzel, H. *J. Raman Spectrosc.* **2001**, *32*, 665.
(32) Lagugné-Labarthet, F.; Buffeteau, T.; Sourisseau, C. *Appl. Phys. B* **2002**, *74*, 129−137.
(33) Lagugné-Labarthet, F.; Buffeteau, T.; Sourisseau, C. *J. Appl. Phys.* **2001**, *90*, 3149.
(34) Fiorini, C.; Prudhomme, N.; de Veyrac, G.; Maurin, I.; Raimond, P.; Nunzi, J. M. *Synth. Met.* **2000**, *115*, 121.
(35) Chaput, F.; Biteau, J.; Lahlil, K.; Boilot, J. P.; Darracq, B.; Levy, Y.; Peretti, J.; Safarov, V. I.; Parent, G.; Fernandez-Acebes, A.; Lehn, J.-M. *Mol. Cryst. Liq. Cryst.* **2000**, *344*, 77.
(36) Frey, L.; Darracq, B.; Chaput, F.; Lahlil, K.; Jonathan, J.-M.; Roosen, G.; Boilot, J. P.; Levy, Y. *Opt. Commun.* **2000**, *173*, 11.
(37) Bublitz, D.; Fleck, B.; Wenke, L. *Appl. Phys. B* **2001**, *72*, 931.
(38) Cipparrone, G.; Mazulla, A.; Russo, G. *Appl. Phys. Lett.* **2001**, *78*, 1186.
(39) Sumaru, K.; Yamanaka, T.; Fukuda, T.; Matsuda, H. *Appl. Phys. Lett.* **1999**, *75*, 1878.
(40) Wu, Y.; Natansohn, A.; Rochon, P. *Macromolecules* **2001**, *34*, 7822.
(41) Zilker, S. J.; Huber, M. R.; Bieringer, T.; Haarer, D. *Appl. Phys. B* **1999**, *68*, 893.
(42) Cimrova, V.; Neher, D.; Kostromine, S. G.; Bieringer, T. *Macromolecules* **1999**, *32*, 8496.
(43) Cimrova, V.; Neher, D.; Hildebrandt, R.; Hegelich, M.; von der Lieth, A.; Marowsky, G.; Hagen, R.; Kostromine, S. G.; Bieringer, T. *Appl. Phys. Lett.* **2002**, *81*, 1228.
(44) Zhang, Y.; Lu, Z.; Deng, X.; Liu, Y.; Zhao, Y. *Opt. Commun.* **2003**, *220*, 289.
(45) Schaller, R. D.; Saykally, R. J.; Shen, Y. R.; Lagugné-Labarthet, F. *Opt. Lett.* **2003**, *28*, 1296.
(46) Lagugné-Labarthet, F.; Buffeteau, T.; Sourisseau, C. *Macromol. Symp.* **1999**, *137*, 75.
(47) Lagugné-Labarthet, F.; Buffeteau, T.; Sourisseau, C. *Appl. Spectrosc.* **2000**, *54*, 699.
(48) Natansohn, A.; Rochon, P.; Gosselin, J.; Xie, S. *Macromolecules* **1992**, *25*, 2268.
(49) Brown, D.; Natansohn, A.; Rochon, P. *Macromolecules* **1995**, *28*, 6116.
(50) Lagugné-Labarthet, F.; Buffeteau, T.; Sourisseau, C. *Phys. Chem. Chem. Phys.* **2002**, *4*, 4020.
(51) Yitzchaik, S.; Berkovic, G.; Krongauz, V. *J. Appl. Phys.* **1991**, *70*, 3949.
(52) Rodriguez, V.; Sourisseau, C. *Nonlinear Opt.* **2000**, *25*, 259.
(53) Rodriguez, V.; Adamietz, F.; Sanguinet, L.; Buffeteau, T.; Sourisseau, C. *J. Nonlinear Opt. Phys. Mater.*, in press.
(54) Rodriguez, V.; Sourisseau, C. *J. Opt. Soc. Am. B* **2002**, *19*, 2650.
(55) Helgert, M.; Fleck, B.; Wenke, L.; Hvilsted, S.; Ramanujam, P. S. *Appl. Phys. B.* **2000**, *70*, 803.
(56) Sekkat, Z.; Dumont, M. *Synth. Met.* **1993**, *54*, 373.
(57) Dumont, M. In *Photoactive Organic Molecules, Science and Applications*; Nato ASI Series; Kajzar, F., Ed.; 1996; Vol. 9, p 501.
(58) Dumont, M.; El Osman, A. *Chem. Phys.* **1999**, *245*, 437.
(59) Lagugné-Labarthet, F.; Sourisseau, C. *New J. Chem.* **1997**, *21*, 879.
(60) Lagugné-Labarthet, F.; Sourisseau, C. *J. Raman Spectrosc.* **1996**, *27*, 491.
(61) Zilker, S. J.; Bieringer, T.; Haarer, D.; Stein, R. S.; VanEgmond, J. W.; Kostromine, S. G. *Adv. Mater.* **1998**, *10*, 855.
(62) Bieringer, T.; Wuttke, R.; Haarer, D.; Gebner, U.; Rübner, J. *Macromol. Chem. Phys.* **1995**, *196*, 1375.
(63) Turrell, G. *J. Raman Spectrosc.* **1984**, *15*, 103.
(64) Brémard, C.; Laureyns, J.; Turrell, G. *Can. J. Spectrosc.* **1987**, *32*, 70.
(65) Turrell, G. In *Practical Raman Sprectroscopies*; Gardinez, D. J., Graves, P. R., Eds.; Springer-Verlag: Berlin, 1989; p 13.
(66) Rodriguez, V.; Adamietz, F.; Sanguinet, L.; Buffeteau, T.; Sourisseau, C. *J. Phys. Chem. B*, in press.
(67) Sourisseau, C.; Maraval, P. *Appl. Spectrosc.* **2003**, *57*, 1324.
(68) Biswas, N.; Umapathy, S. *J. Phys. Chem. A* **2000**, *104*, 2734.
(69) Biswas, N.; Umapathy, S. *J. Raman Spectrosc.* **2001**, *32*, 471.
(70) Berne, B. J.; Pechukas, P.; Harp, G. D. *J. Chem. Phys.* **1968**, *49*, 3125.
(71) Kinosita, K. J.; Kawato, S.; Ikegami, A. *Biophys. J.* **1977**, *20*, 289.
(72) Pottel, H.; Herreman, W.; Van deer Meer, B. W.; Ameloot, M. *Chem. Phys.* **1986**, *102*, 37.
(73) Schaller, R. D.; Saykally, R. J.; Shen, Y. R.; Lagugné-Labarthet, F. In *Organic Photonic Materials and Devices V*; Grote, J. G., Kaino, T., Eds.; Proceedings of SPIE; 2003; Vol. 4991, p 305.